The Canadian Mineralogist
Vol. 48, pp. 1225-1236 (2010)
DOI: 10.3749/canmin.48.5.1225

TEMPERATURE DEPENDENCE OF THE STRUCTURAL PARAMETERS IN THE TRANSFORMATION OF ARAGONITE TO CALCITE, AS DETERMINED FROM *IN SITU* SYNCHROTRON POWDER X-RAY-DIFFRACTION DATA

SYTLE M. ANTAO[§]

Department of Geoscience, University of Calgary, Calgary, Alberta T2N 1N4, Canada

ISHMAEL HASSAN

Department of Chemistry, University of the West Indies, Mona, Kingston 7, Jamaica

ABSTRACT

The temperature dependency of the crystal structure and the polymorphic transition of $CaCO_3$ from aragonite to calcite were studied using Rietveld structure refinement and high-temperature *in situ* synchrotron powder X-ray-diffraction data at ambient pressure, *P*. The orthorhombic metastable aragonite at room *P*, space group *Pmcn*, transforms to trigonal calcite, space group $R\bar{3}c$, at about T_c = 468°C. This transformation occurs rapidly; it starts at about 420°C and is completed by 500°C, an 80°C interval that took about 10 minutes using a heating rate of 8°C/min. Structurally, from aragonite to calcite, the distribution of the Ca atom changes from approximately hexagonal to cubic close-packing. A 5.76% discontinuous increase in volume accompanies the reconstructive first-order transition. Besides the change in coordination of the Ca atom from nine to six from aragonite to calcite, the CO_3 groups change by a 30° rotation across the transition.

Keywords: aragonite, calcite, $CaCO_3$, high-temperature structure, phase transition, Rietveld refinement, X-ray diffraction.

SOMMAIRE

Nous avons étudié la dépendance thermique de la structure cristalline et de la transition polymorphique de $CaCO_3$, de l'aragonite à la calcite, en utilisant des données obtenues par diffraction X sur poudre, acquises *in situ* à température élevée et à pression ambiante avec rayonnement synchrotron. L'aragonite, phase orthorhombique métastable à pression ambiante, groupe spatial *Pmcn*, se transforme en calcite, phase trigonale, groupe spatial $R\bar{3}c$, à environ T_c = 468°C. Cette transformation se déroule rapidement; elle débute à environ 420°C, et elle est complète à 500°C, un intervalle de 80°C qui a pris environ 10 minutes avec un taux de réchauffement de 8°C/min. Du point de vue structural, en allant de l'aragonite à la calcite, la distribution des atomes de Ca change d'un agencement compact aproximativement hexagonal à cubique. Une augmentation discontinue en volume de 5.76% accompagne cette transformation reconstructive de premier ordre. En plus du changement en coordinence de l'atome Ca, de neuf dans l'aragonite à six dans la calcite, les groupes CO_3 font preuve d'une rotation de 30° pendant la transition.

(Traduit par la Rédaction)

Mots-clés: aragonite, calcite, $CaCO_3$, structure à haute température, transition de phase, affinement de Rietveld, diffraction X.

INTRODUCTION

Aragonite is the most common orthorhombic carbonate. It occurs as the inorganic constituent of many invertebrate skeletons (shells of snails, ammonites, clams, corals, sponge spicules, *etc.*) and sediments derived from them. Aragonite is the stable phase at high pressure (*P*) and low temperature (*T*) in the Earth's crust; as such, it occurs as a primary phase in high-*P* blueschist metamorphic rocks. As calcite and aragonite can coexist, both may occur in similar environments. Calcite is important in sedimentary environments and occurs in metamorphic and igneous rocks, as well as in hydrothermal and secondary mineralization.

There is interest in CO_2 sequestration and in the transitions in calcite and aragonite, both $CaCO_3$. Studies on carbonate-group minerals are important in understanding their transition sequences and provide insights

§ *E-mail address*: antao@ucalgary.ca

into the behavior of carbon in the mantle (*e.g.*, Antao *et al.* 2004, Berg 1986, Gillet *et al.* 1993). Aragonite and calcite are of interest because they occur in various geological environments, and the orientational disorder in calcite influences the calcite–aragonite transition, which is used as a geobarometer and geothermometer (Redfern *et al.* 1989, Carlson 1983, Salje & Viswanathan 1976).

The slope of the aragonite–calcite phase boundary varies continuously with a significant change in slope between the low-*T*, low-*P* part and the high-*T*, high-*P* part (Johannes & Puhan 1971). The curvature of the calcite–aragonite coexistence curve was explained by orientational disorder in calcite (Redfern *et al.* 1989). The crystal structure and high-T anion disorder in calcite was recently examined by Antao *et al.* (2009), and the room-*T* structure of aragonite was re-examined by Antao & Hassan (2009).

In this study, we obtained structural parameters with *T* for a well-crystallized sample of aragonite that was heated rapidly (8°C/min) from 25 to 700°C at ambient *P*. The entire experiment took about one hour to complete, including collection of all 40 X-ray-diffraction traces. In addition to unit-cell parameters, we obtained other previously unavailable structural parameters (bond distances and angles) before and after the transition at about T_c = 468°C.

Background Information

At room *P* and *T*, calcite is the thermodynamically stable form, and aragonite exists metastably because of its sluggish conversion rate to calcite. At room *P*, the aragonite-to-calcite transition depends on several factors, such as chemical composition, humidity, presence of calcite nuclei, grain size, and strain (Carlson 1983, Liu & Yund 1993, Lucas *et al.* 1999, Wardecki *et al.* 2008). At ambient *P*, synthetic aragonite transforms to calcite at about 450°C (Lucas *et al.* 1999). Pokroy *et al.* (2007) indicated that structural parameters of biogenic aragonite (mollusc shells) are slightly different from those of well-crystallized aragonite (metamorphic or sedimentary origins) because of the interaction between organic macromolecules and the growing crystallites during biomineralization. Structural differences may also depend on the trace-element (Mg, Sr) content of aragonite.

The thermal-expansion coefficient (TEC) of biogenic aragonite depends on the sample form and origin; powdered biogenic aragonite has the same TEC as aragonite, whereas uncrushed biogenic aragonite has smaller TEC values (Wardecki *et al.* 2008). These authors observed that powdered biogenic aragonite transforms at 280°C, uncrushed biogenic aragonite transforms at 360°C, and aragonite from Atlas Mountains, Morocco, transforms at 450°C, which is the same as that of synthetic aragonite. Under Earth-surface conditions, the transformation of aragonite to calcite in snail shells in governed mainly by time instead of *P* or *T*, and the presence of trace amounts of Mg inhibits this transformation (Sheng *et al.* 2005).

The crystal structure of aragonite was determined by Bragg in 1924 and Wyckoff (1925), and refined by several others (Bevan *et al.* 2002, Caspi *et al.* 2005, Dal Negro & Ungaretti 1971, De Villiers 1971, Dickens & Bowen 1971, Jarosch & Heger 1986). Several high-*P* studies are available for $CaCO_3$, $BaCO_3$ and $SrCO_3$ (Holl *et al.* 2000, Lin & Liu 1997, Ono 2007, Santillan & Williams 2004). Review of studies on calcite and aragonite are given in Reeder (1983), and a Raman spectroscopic study was carried out by Gillet *et al.* (1993). We have recently examined the room-*T* crystal structure of both aragonite, the high-*P* polymorph of $CaCO_3$, and calcite (Antao & Hassan 2009, Antao *et al.* 2009).

In the aragonite structure, layers of nine-coordinated Ca^{2+} cations are parallel to (001), and the atoms occur approximately in the positions of hexagonal close-packing. This is in contrast with the deformed cubic close-packed arrangement of Ca^{2+} cations in calcite, which adopt a sixfold coordination, and gives rise to the pseudohexagonal symmetry in aragonite (Fig. 1). The CO_3 groups are slightly aplanar in aragonite, but planar in calcite.

Experimental

The aragonite sample used in this study, from Cuenca, Spain, occurs as a large (several cm in size) euhedral (hexagonal in shape) crystal; the chemical formula is nearly ideal, $CaCO_3$. This sample is probably from a sedimentary deposit. A room-*T* structure was obtained from Rietveld structure refinement and synchrotron high-resolution powder X-ray-diffraction (HRPXRD) data (Antao & Hassan 2009).

In situ high-*T* synchrotron powder X-ray-diffraction (XRD) experiments were performed at beamline 1-BM, Advanced Photon Source, Argonne National Laboratory. The sample was loaded into a silica glass capillary of diameter 0.7 mm, that was sealed and oscillated during the experiment over a range of 10°. The high-*T* XRD data were collected using monochromatic synchrotron radiation [λ = 0.61684(5) Å] at room pressure and from about 25 to 702°C. The elevated *T* was obtained using a heater and a thermocouple element placed close to the sample. On the basis of calibrations using various standards, the experimental error in *T* is about ±2 K. Data were collected at regular intervals using a heating rate of about 8°C/min to a maximum 2θ of about 30°. The heating experiment and collection of about 40 XRD traces were completed in about one hour. An image plate (IP) detector (Mar345) mounted perpendicular to the beam path was used to collect full-circle Debye–Scherrer rings with an exposure time of 4 s. An external LaB_6 standard was used to determine the sample-to-detector distance, wavelength, and tilt of

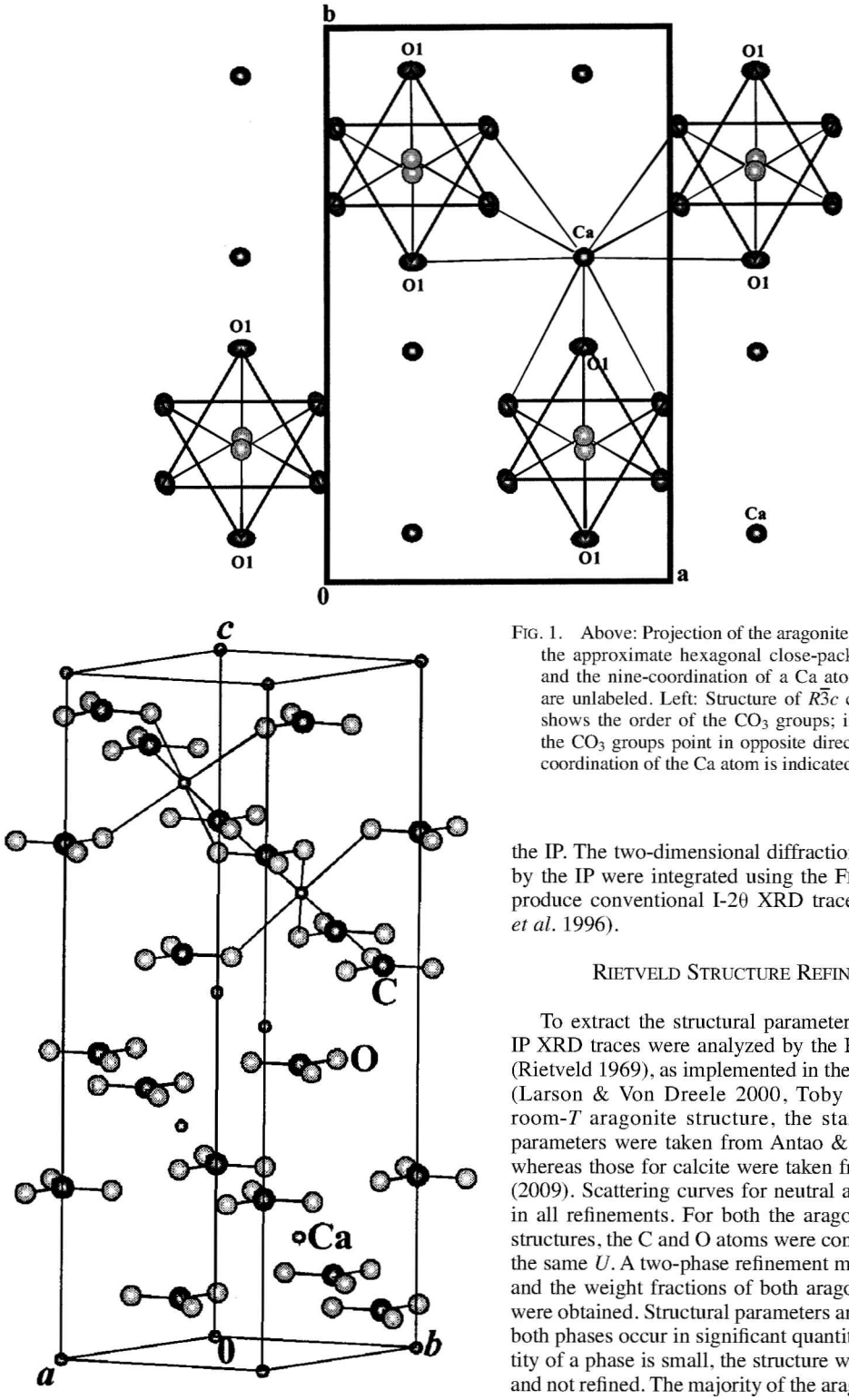

FIG. 1. Above: Projection of the aragonite structure showing the approximate hexagonal close-packing of the atoms and the nine-coordination of a Ca atom. The O2 atoms are unlabeled. Left: Structure of $R\bar{3}c$ calcite: a unit cell shows the order of the CO_3 groups; in adjacent layers, the CO_3 groups point in opposite directions. The sixfold coordination of the Ca atom is indicated.

the IP. The two-dimensional diffraction rings recorded by the IP were integrated using the FIT2D program to produce conventional I-2θ XRD traces (Hammersley *et al.* 1996).

RIETVELD STRUCTURE REFINEMENT

To extract the structural parameters, the measured IP XRD traces were analyzed by the Rietveld method (Rietveld 1969), as implemented in the GSAS program (Larson & Von Dreele 2000, Toby 2001). For the room-*T* aragonite structure, the starting structural parameters were taken from Antao & Hassan (2009), whereas those for calcite were taken from Antao *et al.* (2009). Scattering curves for neutral atoms were used in all refinements. For both the aragonite and calcite structures, the C and O atoms were constrained to have the same *U*. A two-phase refinement method was used, and the weight fractions of both aragonite and calcite were obtained. Structural parameters are reliable where both phases occur in significant quantities. If the quantity of a phase is small, the structure was held constant and not refined. The majority of the aragonite-to-calcite

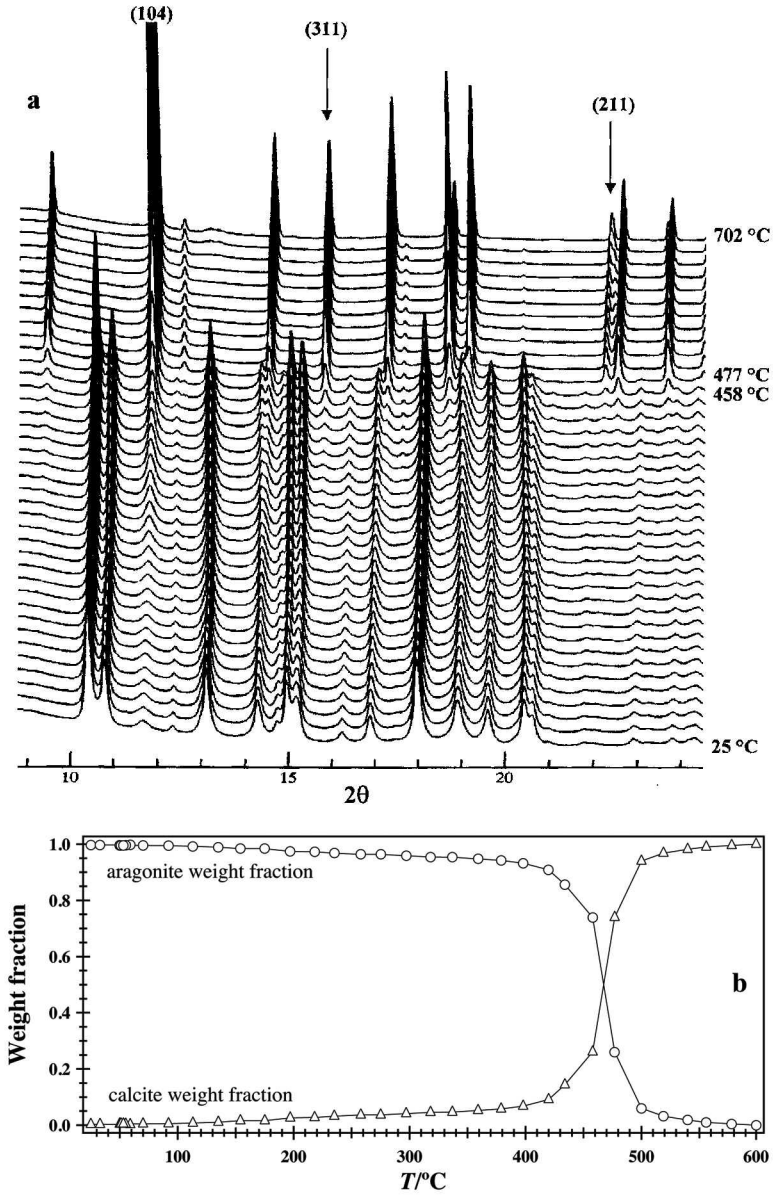

FIG. 2. (a) Stacks of XRD traces showing the transition at T_c = 468°C from aragonite to calcite on heating from 25 to 702°C. The (104), (113) and (211) reflections for calcite are labeled. The strongest peak in calcite, (104) can be seen to develop in aragonite before 468°C. (b) Evolution of the weight fractions for aragonite and calcite with T. The original sample of aragonite contains 0.0032 weight fraction of calcite at room T [only the (104) peak is noticeable]. The transformation from aragonite to calcite occurs in a rapid process (10 minutes) between 420 and 500°C, an 80°C interval.

TABLE 1a. ARAGONITE: UNIT-CELL PARAMETERS, ATOM COORDINATES†, ISOTROPIC DISPLACEMENT PARAMETERS U (Å^2), AND RIETVELD REFINEMENT STATISTICS

T °C	a Å	b Å	c Å	V Å^3	Ca_y	Ca_z	U_{Ca}	C_y	C_z	¨U_C
25	4.9556(4)	7.9779(6)	5.7420(5)	227.01(3)	0.4142(2)	0.7537(5)	0.007(1)	0.7661(14)	-0.0689(13)	0.023(1)
50	4.9566(4)	7.9808(6)	5.7464(5)	227.32(3)	0.4142(2)	0.7538(5)	0.008(1)	0.7663(14)	-0.0684(13)	0.025(1)
70	4.9576(4)	7.9835(6)	5.7503(5)	227.59(3)	0.4141(2)	0.7538(5)	0.008(1)	0.7662(14)	-0.0681(13)	0.026(1)
92	4.9586(4)	7.9867(6)	5.7547(5)	227.90(3)	0.4141(2)	0.7538(5)	0.009(1)	0.7658(14)	-0.0679(13)	0.026(1)
113	4.9594(4)	7.9893(6)	5.7584(5)	228.16(3)	0.4141(2)	0.7537(5)	0.009(1)	0.7662(14)	-0.0677(13)	0.028(1)
135	4.9605(4)	7.9925(6)	5.7629(5)	228.48(3)	0.4139(2)	0.7538(5)	0.010(1)	0.7659(14)	-0.0670(13)	0.028(1)
154	4.9614(4)	7.9954(6)	5.7668(5)	228.76(3)	0.4139(2)	0.7539(5)	0.011(1)	0.7655(14)	-0.0671(13)	0.030(1)
175	4.9624(4)	7.9989(6)	5.7714(5)	229.09(3)	0.4139(2)	0.7538(5)	0.012(1)	0.7645(14)	-0.0668(14)	0.031(1)
197	4.9635(4)	8.0024(6)	5.7760(5)	229.42(3)	0.4137(2)	0.7538(5)	0.013(1)	0.7647(15)	-0.0660(14)	0.033(2)
218	4.9644(4)	8.0057(6)	5.7805(5)	229.74(3)	0.4136(2)	0.7539(5)	0.013(1)	0.7643(15)	-0.0660(14)	0.034(2)
235	4.9653(4)	8.0088(6)	5.7847(5)	230.04(3)	0.4135(2)	0.7542(5)	0.013(1)	0.7642(15)	-0.0653(14)	0.034(2)
258	4.9664(4)	8.0126(6)	5.7898(5)	230.40(3)	0.4134(2)	0.7545(5)	0.014(1)	0.7636(15)	-0.0649(14)	0.035(2)
275	4.9672(4)	8.0157(6)	5.7938(5)	230.68(3)	0.4134(2)	0.7547(5)	0.015(1)	0.7631(15)	-0.0641(14)	0.036(2)
297	4.9683(4)	8.0196(6)	5.7989(5)	231.05(3)	0.4133(2)	0.7550(5)	0.016(1)	0.7633(15)	-0.0634(14)	0.036(2)
318	4.9693(4)	8.0234(6)	5.8037(5)	231.40(3)	0.4132(2)	0.7552(5)	0.017(1)	0.7628(15)	-0.0633(14)	0.036(2)
337	4.9703(4)	8.0272(6)	5.8087(5)	231.75(3)	0.4132(2)	0.7555(5)	0.018(1)	0.7622(15)	-0.0634(15)	0.038(2)
359	4.9713(4)	8.0311(6)	5.8141(5)	232.13(3)	0.4132(2)	0.7559(5)	0.018(1)	0.7618(15)	-0.0615(15)	0.037(2)
379	4.9721(4)	8.0344(6)	5.8183(5)	232.43(3)	0.4132(3)	0.7560(5)	0.019(1)	0.7615(15)	-0.0620(15)	0.038(2)
398	4.9731(4)	8.0384(6)	5.8236(5)	232.81(3)	0.4132(3)	0.7561(5)	0.019(1)	0.7614(15)	-0.0619(15)	0.038(2)
420	4.9744(3)	8.0432(6)	5.8300(4)	233.26(3)	0.4132(3)	0.7563(5)	0.020(1)	0.7615(15)	-0.0617(15)	0.039(2)
434	4.9750(3)	8.0446(5)	5.8329(4)	233.44(3)	0.4133(3)	0.7564(5)	0.020(1)	0.7613(15)	-0.0622(15)	0.039(2)
458	4.9767(3)	8.0486(5)	5.8396(3)	233.91(2)	0.4131(3)	0.7564(5)	0.021(1)	0.7605(15)	-0.0625(15)	0.039(2)
477	4.9778(4)	8.0528(7)	5.8462(4)	234.35(3)	0.4120(5)	0.7553(11)	0.022(3)	0.7535(33)	-0.0593(30)	0.036(3)

† Ca is at (¼,y,z), C is at (¼,y,z), O1 is at (¼,y,z), and O2 is at (x,y,z). ¨ Constraint: $U_{O1} = U_{O2} = U_C$.

TABLE 1a (cont'd). ARAGONITE: UNIT-CELL PARAMETERS, ATOM COORDINATES†, ISOTROPIC DISPLACEMENT PARAMETERS U (Å^2), AND RIETVELD REFINEMENT STATISTICS

T °C	$O1_y$	$O1_z$	$O2_x$	$O2_y$	$O2_z$	*R_F^2
25	0.9186(9)	-0.0898(7)	0.4733(9)	0.6839(5)	-0.0987(7)	0.0315
50	0.9188(9)	-0.0900(7)	0.4734(9)	0.6835(5)	-0.0987(7)	0.0323
70	0.9187(9)	-0.0896(7)	0.4733(10)	0.6837(5)	-0.0983(7)	0.0320
92	0.9183(9)	-0.0889(7)	0.4735(10)	0.6840(5)	-0.0983(7)	0.0323
113	0.9188(9)	-0.0891(7)	0.4733(10)	0.6838(5)	-0.0984(7)	0.0330
135	0.9184(9)	-0.0887(7)	0.4730(10)	0.6841(5)	-0.0982(7)	0.0329
154	0.9184(9)	-0.0879(7)	0.4731(10)	0.6844(5)	-0.0981(7)	0.0331
175	0.9179(9)	-0.0884(7)	0.4738(10)	0.6843(5)	-0.0981(7)	0.0338
197	0.9184(9)	-0.0876(7)	0.4734(11)	0.6844(5)	-0.0982(7)	0.0339
218	0.9184(9)	-0.0875(7)	0.4732(11)	0.6845(5)	-0.0982(8)	0.0341
235	0.9189(9)	-0.0870(7)	0.4731(11)	0.6848(5)	-0.0983(8)	0.0338
258	0.9190(9)	-0.0863(7)	0.4726(11)	0.6853(5)	-0.0983(8)	0.0352
275	0.9193(9)	-0.0865(7)	0.4726(11)	0.6853(5)	-0.0981(8)	0.0350
297	0.9198(9)	-0.0860(8)	0.4721(11)	0.6856(5)	-0.0981(8)	0.0350
318	0.9198(9)	-0.0852(8)	0.4719(11)	0.6860(5)	-0.0978(8)	0.0359
337	0.9194(9)	-0.0846(8)	0.4718(11)	0.6860(5)	-0.0975(8)	0.0368
359	0.9197(9)	-0.0847(8)	0.4715(11)	0.6863(5)	-0.0976(8)	0.0378
379	0.9196(9)	-0.0842(8)	0.4716(11)	0.6865(5)	-0.0976(8)	0.0394
398	0.9196(9)	-0.0838(8)	0.4713(11)	0.6866(5)	-0.0974(8)	0.0408
420	0.9194(9)	-0.0837(8)	0.4709(11)	0.6865(5)	-0.0968(8)	0.0425
434	0.9195(9)	-0.0839(8)	0.4707(11)	0.6865(5)	-0.0968(8)	0.0438
458	0.9186(10)	-0.0845(8)	0.4701(12)	0.6865(6)	-0.0963(8)	0.0468
477	0.9128(20)	-0.0860(17)	0.4699(25)	0.6879(11)	-0.0976(17)	0.0538

* R_F^2 = R structure factor based on observed and calculated structure-amplitudes = $[\Sigma(F_o^2 - F_c^2)/\Sigma(F_o^2)]^{1/2}$.

TABLE 1b. ARAGONITE: SELECTED BOND-DISTANCES (Å) AND ANGLES (°)

T °C	Ca-O1 ×1	Ca-O1 ×2	Ca-O2 ×2	Ca-O2 ×2	Ca-O2 ×2	<Ca-O>	C-O1 ×1	C-O2 ×2	<C-O>	O1-C-O2 ×2	O2-C-O2 ×1	<O-C-O>
25	2.381(5)	2.651(2)	2.563(4)	2.533(6)	2.460(5)	2.533	1.223(10)	1.297(6)	1.272	119.4(5)	117.0(10)	118.6
50	2.383(5)	2.651(2)	2.562(4)	2.533(6)	2.463(5)	2.533	1.224(10)	1.301(6)	1.275	119.4(5)	116.7(10)	118.5
70	2.383(5)	2.653(2)	2.565(4)	2.533(6)	2.463(5)	2.535	1.224(10)	1.299(6)	1.274	119.4(5)	116.8(10)	118.5
92	2.384(5)	2.655(2)	2.569(4)	2.534(6)	2.462(5)	2.536	1.224(10)	1.298(6)	1.273	119.2(5)	117.2(10)	118.5
113	2.384(5)	2.655(2)	2.568(4)	2.537(6)	2.463(5)	2.537	1.225(10)	1.300(6)	1.275	119.3(5)	116.8(10)	118.5
135	2.386(5)	2.657(2)	2.571(4)	2.538(6)	2.463(5)	2.538	1.226(10)	1.298(6)	1.274	119.1(5)	117.0(10)	118.4
154	2.384(5)	2.659(2)	2.575(4)	2.539(6)	2.462(5)	2.539	1.228(10)	1.295(6)	1.273	119.0(5)	117.4(11)	118.5
175	2.390(5)	2.659(2)	2.577(4)	2.539(6)	2.462(5)	2.540	1.234(11)	1.295(6)	1.275	118.6(5)	118.0(11)	118.4
197	2.386(5)	2.661(2)	2.580(4)	2.541(6)	2.461(5)	2.541	1.236(11)	1.295(7)	1.275	118.6(5)	117.8(11)	118.3
218	2.388(5)	2.663(2)	2.581(4)	2.543(6)	2.463(5)	2.543	1.239(11)	1.293(7)	1.275	118.5(5)	118.0(11)	118.3
235	2.387(6)	2.665(2)	2.584(4)	2.544(6)	2.461(5)	2.544	1.245(11)	1.291(7)	1.276	118.4(5)	118.1(11)	118.3
258	2.387(6)	2.668(2)	2.587(4)	2.547(6)	2.462(5)	2.546	1.252(11)	1.286(7)	1.275	118.1(5)	118.6(11)	118.3
275	2.389(6)	2.668(2)	2.589(4)	2.546(6)	2.462(5)	2.547	1.258(11)	1.285(7)	1.276	117.8(5)	118.8(11)	118.1
297	2.388(6)	2.671(2)	2.590(4)	2.548(6)	2.464(5)	2.548	1.261(11)	1.283(7)	1.276	117.8(5)	118.6(11)	118.1
318	2.387(6)	2.674(2)	2.595(4)	2.549(6)	2.463(5)	2.550	1.266(11)	1.279(7)	1.275	117.6(5)	119.1(11)	118.1
337	2.390(6)	2.677(2)	2.596(4)	2.548(7)	2.466(5)	2.551	1.268(11)	1.276(7)	1.273	117.5(5)	119.5(11)	118.2
359	2.392(6)	2.678(2)	2.597(4)	2.550(7)	2.467(5)	2.553	1.276(11)	1.274(7)	1.275	117.1(5)	119.5(11)	117.9
379	2.392(6)	2.680(2)	2.600(4)	2.551(7)	2.467(5)	2.554	1.277(11)	1.273(7)	1.274	117.0(6)	119.9(11)	118.0
398	2.393(6)	2.682(2)	2.601(4)	2.552(7)	2.469(5)	2.556	1.278(11)	1.271(7)	1.273	117.0(5)	119.9(11)	118.0
420	2.396(6)	2.683(2)	2.603(4)	2.552(7)	2.473(5)	2.558	1.276(11)	1.270(7)	1.272	117.1(6)	119.8(11)	118.0
434	2.399(6)	2.684(2)	2.603(4)	2.553(7)	2.474(5)	2.558	1.279(11)	1.268(7)	1.272	117.1(6)	119.9(11)	118.0
458	2.408(6)	2.683(2)	2.605(5)	2.554(7)	2.478(5)	2.561	1.279(11)	1.262(7)	1.268	117.0(6)	120.4(12)	118.1
477	2.444(9)	2.678(5)	2.622(9)	2.568(9)	2.460(9)	2.567	1.292(19)	1.236(11)	1.255	113.7(9)	124.7(15)	117.4

TABLE 2. $R\bar{3}c$ CALCITE: CELL PARAMETERS, BOND DISTANCES (Å), ISOTROPIC DISPLACEMENT PARAMETERS U, ATOM COORDINATES†, AND RIETVELD REFINEMENT STATISTICS

T °C	a Å	c Å	V Å^3	Ca–O ×6	C–O ×3	U_{Ca}	$^*U_C$	x_{O1}	R_F^2
297	4.980(2)	17.192(8)	369.3(2)	2.352(7)	1.30(1)	0.005(6)	0.065(10)	0.261(3)	0.0350
318	4.978(2)	17.211(7)	369.3(2)	2.351(6)	1.30(1)	0.006(6)	0.062(9)	0.262(3)	0.0359
337	4.976(2)	17.227(7)	369.4(2)	2.350(6)	1.31(1)	0.006(6)	0.055(9)	0.262(2)	0.0368
359	4.974(1)	17.243(6)	369.5(2)	2.349(6)	1.31(1)	0.010(5)	0.055(8)	0.263(2)	0.0378
379	4.974(1)	17.251(5)	369.6(2)	2.351(5)	1.30(1)	0.012(5)	0.054(8)	0.262(2)	0.0394
398	4.974(1)	17.261(4)	369.8(1)	2.354(5)	1.300(9)	0.013(4)	0.052(7)	0.261(2)	0.0408
420	4.9748(7)	17.270(3)	370.2(1)	2.357(4)	1.295(8)	0.0173(34)	0.050(5)	0.260(2)	0.0425
434	4.9757(5)	17.273(2)	370.33(7)	2.363(3)	1.284(5)	0.0200(23)	0.048(4)	0.258(1)	0.0438
458	4.9766(3)	17.284(1)	370.70(4)	2.371(2)	1.271(3)	0.0238(13)	0.047(2)	0.2554(6)	0.0468
477	4.9775(1)	17.2949(6)	371.08(2)	2.3780(7)	1.259(1)	0.0274(6)	0.0476(9)	0.2529(3)	0.0538
500	4.9775(1)	17.3105(5)	371.42(2)	2.3803(6)	1.256(1)	0.0310(5)	0.0518(8)	0.2523(3)	0.0633
519	4.9773(1)	17.3231(5)	371.66(2)	2.3819(6)	1.254(1)	0.0333(5)	0.0552(8)	0.2519(3)	0.0661
540	4.9771(1)	17.3369(5)	371.92(2)	2.3833(7)	1.252(1)	0.0348(5)	0.0577(9)	0.2516(3)	0.0686
556	4.9769(1)	17.3479(5)	372.14(2)	2.3842(7)	1.251(1)	0.0359(5)	0.0598(9)	0.2515(3)	0.0697
578	4.9767(1)	17.3610(5)	372.39(2)	2.3854(7)	1.250(1)	0.0357(6)	0.061(1)	0.2512(3)	0.0729
599	4.9766(1)	17.3757(5)	372.68(2)	2.3868(7)	1.249(1)	0.0372(7)	0.063(1)	0.2509(3)	0.0729
620	4.9764(1)	17.3886(5)	372.93(2)	2.3881(7)	1.247(1)	0.0384(7)	0.066(1)	0.2507(3)	0.0799
644	4.9761(1)	17.4163(5)	373.49(2)	2.3911(7)	1.244(1)	0.0401(7)	0.070(1)	0.2500(3)	0.0867
662	4.9759(1)	17.4316(5)	373.78(2)	2.3926(8)	1.243(2)	0.0408(8)	0.072(1)	0.2497(3)	0.0921
681	4.9759(1)	17.4486(5)	374.13(2)	2.3947(8)	1.240(2)	0.0419(8)	0.074(1)	0.2492(3)	0.0982
702	4.9742(1)	17.4676(5)	374.29(2)	2.3959(8)	1.238(2)	0.0420(9)	0.077(1)	0.2490(3)	0.0990

† Ca is at (0,0,0), C is at (0,0,¼), O1 is at (x,0,¼). * Constraint: $U_C = U_O$, in Å^2.

transformation occurs between 458 to 477°C, so we consider T_c equal to 468°C (Figs. 2a, b).

The background for each trace was modeled with a Chebyschev polynomial (16 terms). The reflection-peak profiles were fitted using type-3 profile in the GSAS program. A full-matrix least-squares refinement was carried out by varying a scale factor, cell parameters, zero shift, atom coordinates, and U. Near the end of the refinement, all parameters were allowed to vary simultaneously, and the refinement proceeded to convergence. The number of observed reflections in a typical XRD trace was about 123 for aragonite and 34 for the $R\bar{3}c$ calcite. Synchrotron powder XRD traces are shown in Figures 2a and 3, as examples. Structural parameters for aragonite are given in Tables 1a and 1b, and those for calcite, in Table 2.

An improvement to the data in this study may be obtained using single-crystal X-ray-diffraction data to provide anisotropic displacement parameters (ADPs). Synchrotron powder XRD data are obtained rapidly on a fine T scale, but ADPs are not reliable.

Results and Discussion

Structure of aragonite and $R\bar{3}c$ calcite

The idealized structure of aragonite has an approximate hexagonal close-packing, with the C atoms of the CO_3 groups projecting nearly on top of each other (Fig. 1a). The Ca atom is coordinated by nine oxygen atoms of six different CO_3 groups that are slightly aplanar. Further details on the aragonite structure are discussed elsewhere (Antao & Hassan 2009).

In calcite, the CO_3 groups are planar and occur in layers perpendicular to the **c** axis (Fig. 1b). The CO_3 groups in one layer have identical orientation, whereas those in adjacent layers are rotated by 180° with respect to the other. The coordination for the Ca atom is six. We have used this model for the calcite structure to 702°C. At higher T, the CO_3 groups disorder in calcite, and a different structural model is necessary (Antao *et al.* 2008, 2009).

From the stack of XRD traces at different T and the weight fractions, the bulk of the transition from aragonite to calcite occurs at about T_c = 468°C, between 458 and 477°C (Figs. 2a, b). The trace at 25°C contains a minor amount of "seed" calcite (0.0032 wt. fraction, or 0.32%). In the weight-fraction plot, major changes occur between 420 and 500°C (Fig. 2b). In this 80°C interval, the aragonite changes to calcite in a very rapid process that took about 10 minutes, as the heating rate was 8°C /min. In the traces above 702°C, a few diffraction peaks from CaO arise from the breakdown of calcite (not shown). Examples of traces from the Rietveld refinement of the aragonite and calcite structure at different T are given (Fig. 3).

Our aragonite sample has a T_c of 468°C when heated at a continuous rate of 8°C/min. and obtaining each XRD trace in regular four-second exposures. For synthetic aragonite, T_c is equal to 450°C if heated at a rate of 0.42°C/min. (Lucas *et al.* 1999). For an aragonite sample from the Atlas Mountains, Serfou, Morocco, T_c is equal to 450°C (Wardecki *et al.* 2008). Figure 2a is similar to that shown by Lucas *et al.* (1999), and our room-T X-ray trace indicates a minor amount of calcite (0.32%) in the bulk aragonite sample, based on refined weight-fractions (Fig. 2b). The traces from Lucas *et al.* (1999) also indicate a small amount of calcite in their synthetic sample.

Wardecki *et al.* (2008) reported that powdered biogenic aragonite transforms at 280°C, uncrushed biogenic aragonite transforms at 360°C, and aragonite from the Atlas Mountains transforms at 450°C. The bulk of our aragonite sample transforms at 468°C (Fig. 2). The difference in T_c between well-crystallized aragonite and biogenic aragonite is probably related to grain size, with the nanosized crystals in poorly crystallized biogenic aragonite transforming at a lower T than well-crystallized aragonite from sedimentary or metamorphic environments. A small amount of "seed" calcite in aragonite may be necessary to stabilize aragonite under ambient conditions and helps initiate the transformation on heating. Pure aragonite may transform to calcite at a higher temperature than 468°C.

The room-T structural parameters for aragonite obtained from the present IP XRD and HRPXRD datasets are similar to each other, but that obtained by the superior HRPXRD data is more accurate than the IP XRD data (Antao & Hassan 2009). However, the close similarity between the two datasets at room T gives us confidence that detailed structural changes can be obtained at high T using the present IP XRD data.

Unit-cell parameters for aragonite and calcite with T

The room-T unit-cell parameters for calcite and aragonite are discussed elsewhere (Antao & Hassan 2009, Antao *et al.* 2009). The variations of the unit-cell parameters with T for both aragonite and calcite are shown (Figs. 4, 5). The room-T cell parameters for aragonite are nearly identical to those obtained by HRPXRD data, except for the a parameter, which is slightly different (4.956 compared to 4.962 Å; Fig. 4a). This small difference arises from the number of reflections used in the refinements and also the different resolutions in the two experimental techniques. In general, the variation of the unit-cell parameters of aragonite increases approximately linearly to 468°C. Linear increases in cell parameters for aragonite were obtained by Lucas *et al.* (1999), except that their $\boldsymbol{a}$ parameter variation was found to be non-linear. Wardecki *et al.* (2008) obtained similar variation in cell parameters for their aragonite samples. In Figure 4a, the a unit-cell parameter for calcite contracts and becomes nearly identical to the a parameter of aragonite, so the transformation probably began as an oriented intergrowth

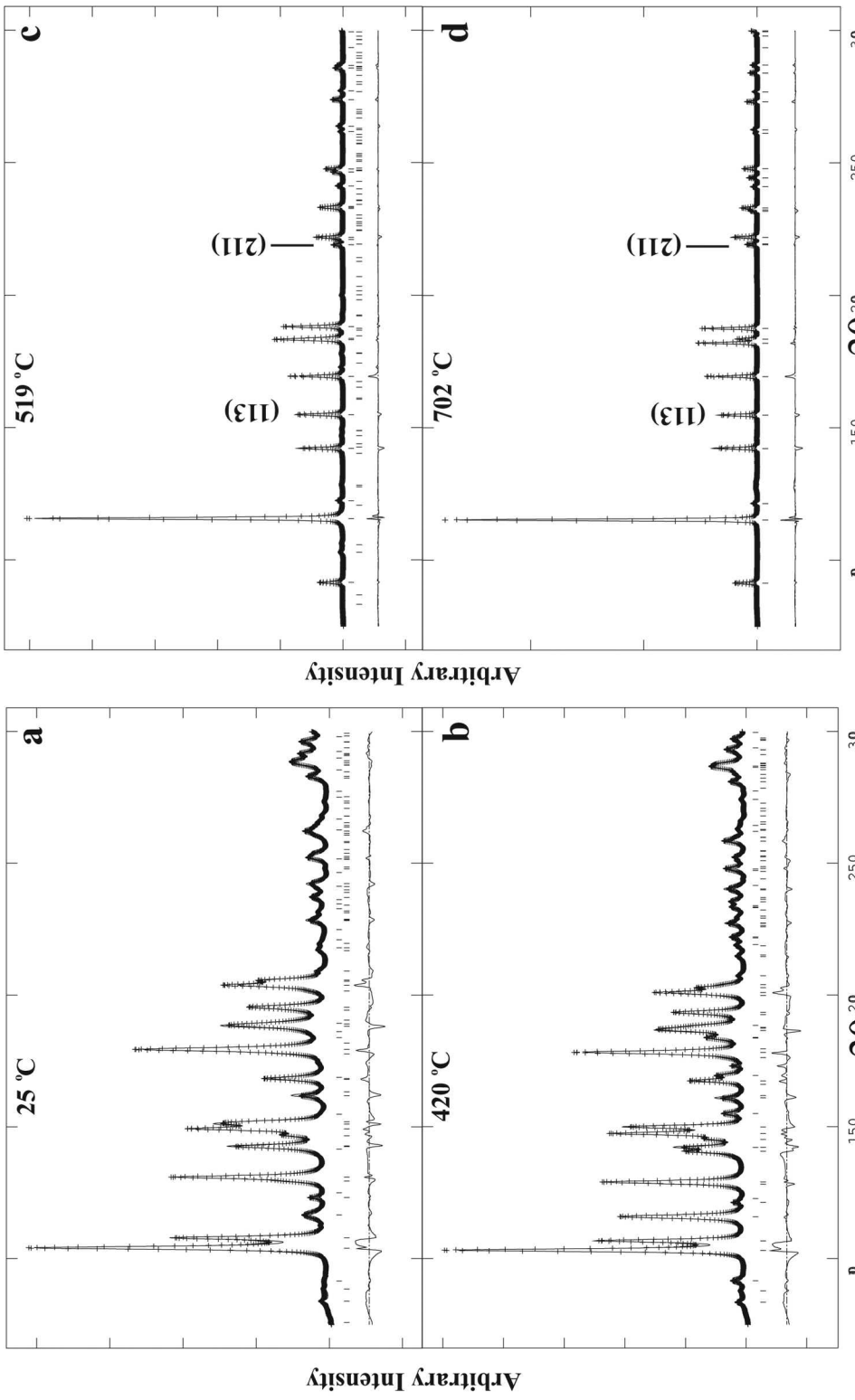

FIG. 3. Comparison of the XRD traces for aragonite (with minor calcite) at (a) 25°C and (b) 420°C, and for calcite at (c) 519°C (contains minor aragonite) and (d) 702°C (pure calcite), together with the calculated (continuous line) and observed (crosses) profiles. The difference curve ($I_{obs} - I_{calc}$) is shown at the bottom. The short vertical lines indicate positions of the allowed reflections. Reflections (113) and (211) are indicated for calcite.

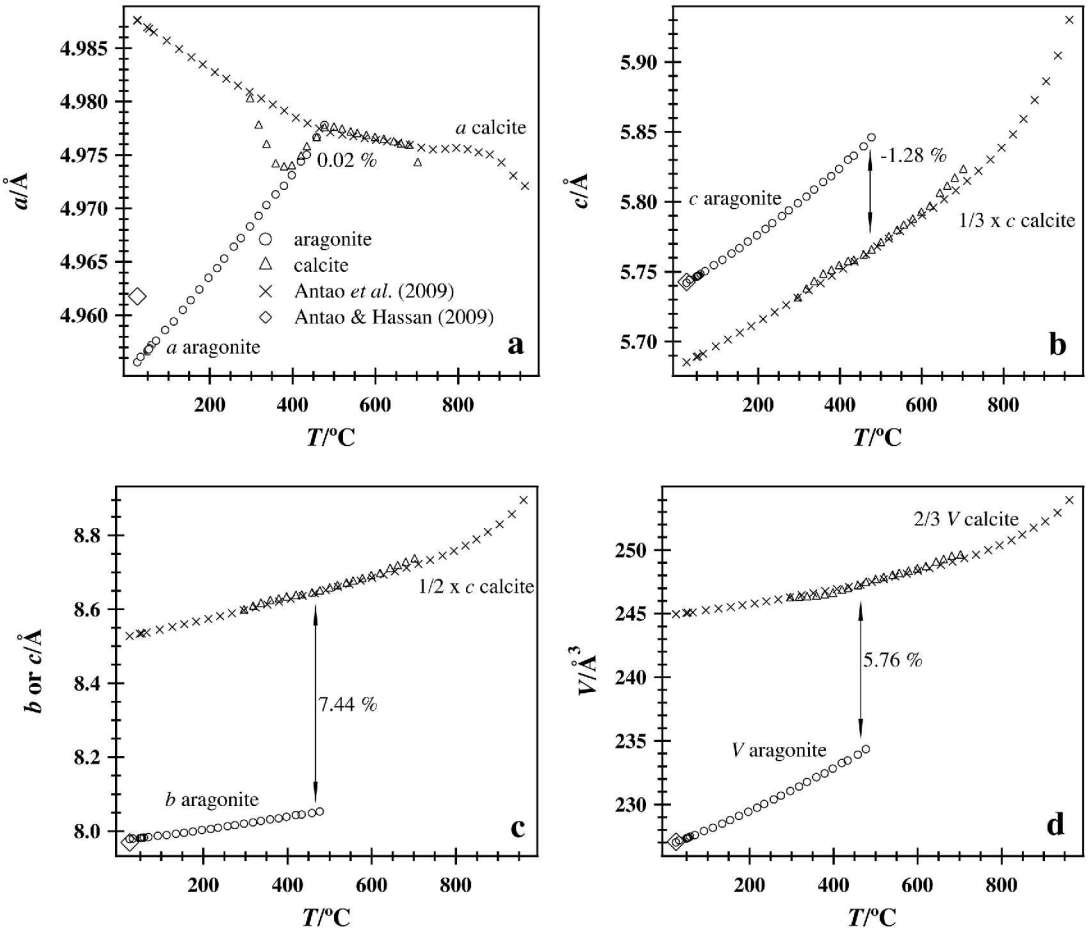

FIG. 4. Temperature variation of the unit-cell parameters for aragonite and calcite: (a) a, (b) c, (c) b or c, (d) V. The errors are smaller than the symbols. Cell parameters for calcite from Antao *et al.* (2009) are included for comparison (× symbol) in Figures 4 to 6. The a cell parameter shows a negative thermal-expansion effect for calcite.

on the (100) plane of aragonite. Data from Antao *et al.* (2009) for calcite are included for comparison (shown as × symbols in Figs. 4, 5, 6b). At the transition, the percentage change in unit-cell parameters is given (Fig. 4). The volume increases by 5.76% (Fig. 4d).

When all the axial and volume expansions of the unit-cell parameters are normalized to that of aragonite data at room T and plotted as a function of T, in the case of aragonite the expansion for the **c** axis is largest, followed by the **b** axis, and the **a** axis is the least (Fig. 5). The expansion of the calcite structure is strongly anisotropic, with the axial expansion along the **c** axis (normal to the CO_3 groups) being considerably larger than that along the **a** axis. A slight negative thermal-expansion effect is observed for the **a** axis in calcite. The a/a_0 ratio for both aragonite and calcite are nearly the same at all T (Fig. 5).

The volume thermal expansion for aragonite was obtained by fitting all the cell-volume data simultaneously to the expression:

$$V(T) = V_{Tr} \exp\left[\int_{Tr}^{T} \alpha_V(T)\,dT\right]$$

where $V(T)$ is the volume at any temperature T, V_{Tr} is the volume at reference T, and $a_V(T)$ is a polynomial expression for the volume thermal-expansion coefficient (TEC): $\alpha_V(T) = a_0 + a_1 T$. The values: $a_0 = 5.47\ (\pm 0.04) \times 10^{-5}$ and $a_1 = 6.12\ (\pm 0.19) \times 10^{-8}$ were obtained with V_{Tr} = 227.01(3) Å^3 at 25°C. A larger range of high-T structural data for calcite is given in Antao *et al.* (2009), and these data are included in Figures 4, 5, and 6b. In

that paper, the TEC for calcite was discussed, and is not considered here.

Variation in structural parameters with T

The CO_3 group is expected to behave as a rigid body, so large variations are not expected for the C–O distances with T. The C–O distances obtained from the structure refinement correspond to the distance between refined average coordinates of the atoms, and they contain the effects from thermal and arc motions. The real instantaneous C–O distance is unlikely to change much with T. In aragonite, the <C–O> distance is nearly constant with T, whereas for calcite, it decreases slightly (Fig. 6). These values are reliable only where a phase occurs in a significant quantity, so that many diffraction peaks are available to refine the structure properly. The hump observed for the C–O distance in calcite before T_c may not be significant (Fig. 6a). In aragonite, the average <Ca–O> distance increases slightly with T and is larger than those in calcite because of the nine-coordinated Ca atom in aragonite compared to the six-coordinated Ca atom in calcite (Fig. 6b). For calcite, the average <Ca–O> distance increases slightly with T, and a kink is observed near T_c. The isotropic displacement parameters (U) for the atoms increase with T, as expected (Fig. 6c).

From aragonite to calcite, the distribution of the Ca atom changes from approximately hexagonal to cubic close-packing. The spacing of the low-index planes, for example, the (100) planes, or ***a*** axes, in both calcite and aragonite are related, so an orientational relation exists for the two phases, which aids in the transformation process (Fig. 4). Nine-coordinated Ca atom and higher density occurs in the high-P aragonite phase, whereas six-coordinated Ca atom and lower density occurs in low-P calcite phase. A 5.76% discontinuous increase in volume occurs for this reconstructive first-order transition (Fig. 4d). Besides the change of the Ca atom coordination from nine to six from aragonite to calcite, there is a 30° rotation in the orientation of the CO_3 group across the transition (Fig. 1).

Acknowledgements

We thank one anonymous reviewer, M. Gregorkiewitz and Associate Editor Marcello Mellini for

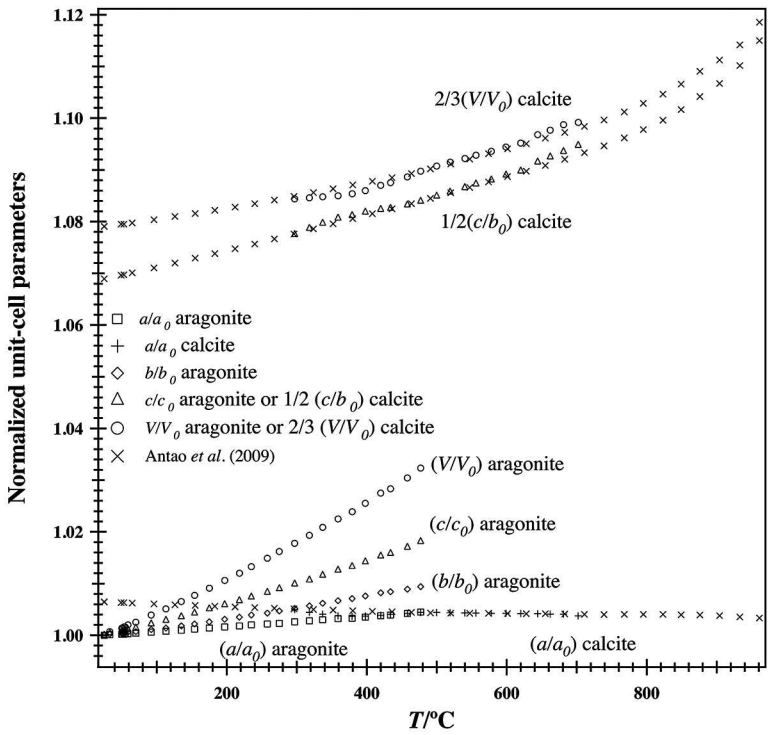

FIG. 5. Variation of the normalized unit-cell parameters with those of aragonite parameters (a_0, b_0, c_0 and V_0) at room T, and plotted as a function of T. For calcite, the a/a_0 ratio contracts slightly, and a larger expansion occurs for the **c** axis. The expansion of the aragonite cell parameters to T_c is nearly linear. The a/a_0 parameter for both minerals nearly coincides with each other.

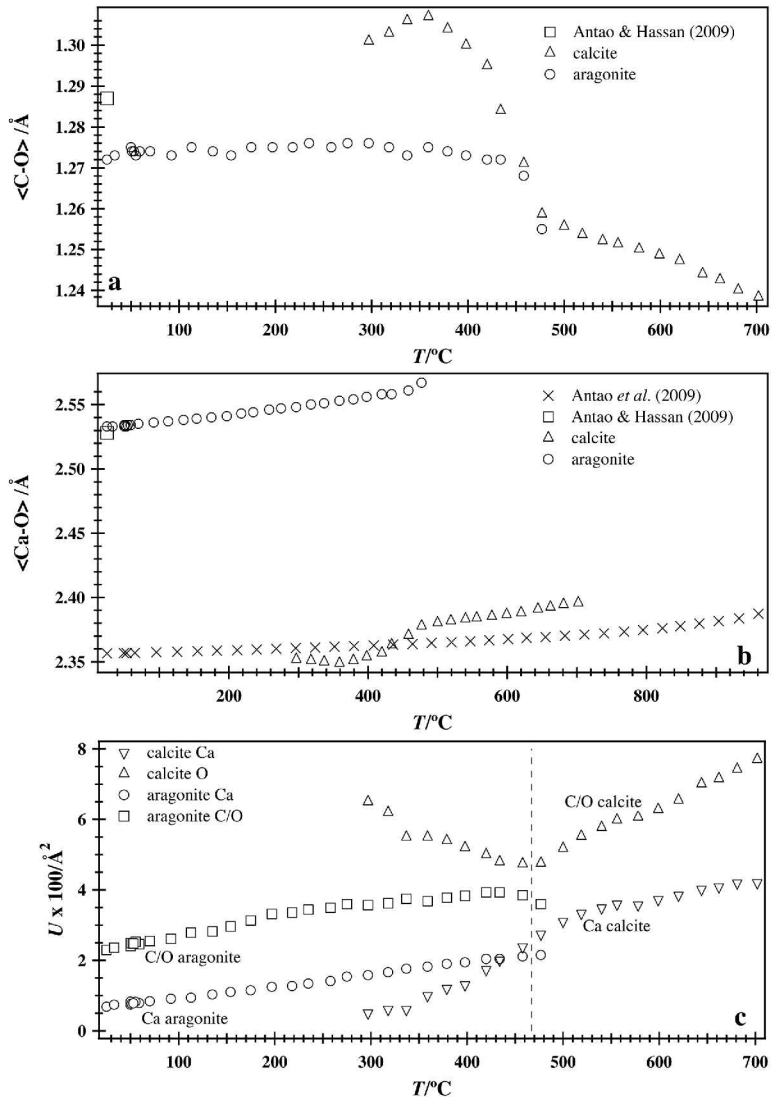

FIG. 6. Variation of structural parameter with T for both aragonite and calcite. (a) Average <C–O> distance, (b) average <Ca–O> distance, and (c) isotropic displacement parameter (U).

constructive and useful comments. The Editor, R.F. Martin, is thanked for his insights and suggestions. The XRD data were collected at the X-ray Operations and Research beamline 1-BM, Advanced Photon Source, Argonne National Laboratory. Use of the Advanced Photon Source was supported by the U.S. Department of Energy, Office of Science, Office of Basic Energy Sciences, under Contract No. DE–AC02–06CH11357. This work was supported by a University of Calgary grant, a Discovery grant from the Natural Sciences and Engineering Research Council of Canada, and an Alberta Ingenuity New Faculty Award to SMA.

REFERENCES

ANTAO, S.M. & HASSAN, I. (2009): The orthorhombic structure of $CaCO_3$, $SrCO_3$, $PbCO_3$, and $BaCO_3$: linear structural trends. *Can. Mineral.* **47**, 1245-1255.

ANTAO, S.M., HASSAN, I., MULDER, W.H. & LEE, P.L. (2008): The $R\bar{3}c \rightarrow R\bar{3}m$ transition in nitratine, $NaNO_3$ and impli-

cations for calcite, $CaCO_3$. *Phys. Chem. Minerals* **35**, 545-557.

ANTAO, S.M., HASSAN, I., MULDER, W.H., LEE, P.L. & TOBY, B.H. (2009): In situ study of the $R\bar{3}c \rightarrow R\bar{3}m$ orientational disorder in calcite. *Phys. Chem. Minerals* **36**, 159-169.

ANTAO, S.M., MULDER, W.H., HASSAN, I., CRICHTON, W. & PARISE, J.B. (2004): Cation disorder in dolomite, $CaMg(CO_3)_2$, and its influence on the aragonite + magnesite → dolomite reaction boundary. *Am. Mineral.* **89**, 1142-1147.

BERG, G.W. (1986): Evidence for carbonate in the mantle. *Nature* **324**, 50-51.

BEVAN, D.J.M., ROSSMANITH, E., MYLREA, D.K., NESS, S.E., TAYLOR, M.R. & CUFF, C. (2002): On the structure of aragonite – Lawrence Bragg revisited. *Acta Crystallogr.* **B58**, 448-456.

BRAGG, W.L. (1924): The structure of aragonite. *Proc. R. Soc. London* **A105**, 16-37.

CARLSON, W.D. (1983): The polymorphs of $CaCO_3$ and the aragonite–calcite transformation. *In* Carbonates: Mineralogy and Chemistry (R.J. Reeder, ed.). *Rev. Mineral.* **11**, 191-225.

CASPI, E.N., POKROY, B., LEE, P.L., QUINTANA, J.P. & ZOLOTOYABKO, E. (2005): On the structure of aragonite. *Acta Crystallogr.* **B61**, 129-132.

DAL NEGRO, A. & UNGARETTI, L. (1971): Refinement of crystal structure of aragonite. *Am. Mineral.* **56**, 768-772.

DE VILLIERS, J.P.R. (1971): Crystal structures of aragonite, strontianite, and witherite. *Am. Mineral.* **56**, 758-767.

DICKENS, B. & BOWEN, J.S. (1971): Refinement of the crystal structure of the aragonite phase of $CaCO_3$. *J. Res. Nat. Bureau Stand.* **A75**, 27-32.

GILLET, P., BIELLMANN, C., REYNARD, B. & MCMILLAN, P. (1993): Raman spectroscopic studies of carbonates. I. High-pressure and high-temperature behaviour of calcite, magnesite, dolomite and aragonite. *Phys. Chem. Minerals* **20**, 1-18.

HAMMERSLEY, A.P., SVENSSON, S.O., HANFLAND, M., FITCH, A.N. & HAUSERMANN, D. (1996): Two-dimensional detector software: from real detector to idealised image to two-theta scan. *High Pressure Res.* **14**, 235-248.

HOLL, C.M., SMYTH, J.R., LAUSTSEN, H.M.S., JACOBSEN, S.D. & DOWNS, R.T. (2000): Compression of witherite to 8 GPa and the crystal structure of $BaCO_3$II. *Phys. Chem. Minerals* **27**, 467-473.

JAROSCH, D. & HEGER, G. (1986): Neutron diffraction refinement of the crystal structure of aragonite. *Tschermaks Mineral. Petrogr. Mitt.* **35**, 127-131.

JOHANNES, W. & PUHAN, D. (1971): The calcite–aragonite transition, reinvestigated. *Contrib. Mineral. Petrol.* **31**, 28-38.

LARSON, A.C. & VON DREELE, R.B. (2000): General Structure Analysis System (GSAS). *Los Alamos National Lab., Rep.* **LAUR 86-748**.

LIN, C.C. & LIU, L.G. (1997): High pressure phase transformations in aragonite-type carbonates. *Phys. Chem. Minerals* **24**, 149-157.

LIU, M. & YUND, R.A. (1993): Transformation kinetics of polycrystalline aragonite to calcite: new experimental data, modelling, and implications. *Contrib. Mineral. Petrol.* **114**, 465-478.

LUCAS, A., MOUALLEM-BAHOUT, M., CAREL, C., GAUDÉ, J. & MATECKI, M. (1999): Thermal expansion of synthetic aragonite condensed review of elastic properties. *J. Solid State Chem.* **146**, 73-78.

ONO, S. (2007): New high-pressure phases in $BaCO_3$. *Phys. Chem. Minerals* **34**, 215-221.

POKROY, B., FIERAMOSCA, J.S., VON DREELE, R.B., FITCH, A.N., CASPI, E.N. & ZOLOTOYABKO, E. (2007): Atomic structure of biogenic aragonite. *Chem. Materials* **19**, 3244-3251.

REDFERN, S.A.T., SALJE, E. & NAVROTSKY, A. (1989): High-temperature enthalpy at the orientational order–disorder transition in calcite – implications for the calcite–aragonite phase-equilibrium. *Contrib. Mineral. Petrol.* **101**, 479-484.

REEDER, R.J., ed. (1983): Carbonates: Mineralogy and Chemistry. *Rev. Mineral.* **11**.

RIETVELD, H.M. (1969): A profile refinement method for nuclear and magnetic structures. *Appl. Crystallogr.* **2**, 65-71.

SALJE, E. & VISWANATHAN, K. (1976): Phase-diagram calcite–aragonite as derived from crystallographic properties. *Contrib. Mineral. Petrol.* **55**, 55-67.

SANTILLAN, J. & WILLIAMS, Q. (2004): A high pressure X-ray diffraction study of aragonite and the post-aragonite phase transition in $CaCO_3$. *Am. Mineral.* **89**, 1348-1352.

SHENG XUEFEN, CHEN JUN, CAI YUANFENG, CHEN YANG & JI JUNFENG (2005): Aragonite–calcite transformation in fossil snail shells of loess sequence in Loess Plateau, central China. *Chinese Sci. Bull.* **50**, 891-895.

TOBY, B.H. (2001): EXPGUI, a graphical user interface for GSAS. *J. Appl. Crystallogr.* **34**, 210-213.

WARDECKI, D., PRZENIOSLO, R. & BRUNELLI, M. (2008): Internal pressure in annealed biogenic aragonite. *Crystal Eng. Comm.* **10**, 1450-1453.

WYCKOFF, R.W.G. (1925): Orthorhombic space group criteria and their applications to aragonite. *Am. J. Sci.* **209**, 145-175.

Received August 5, 2009, revised manuscript accepted September 18, 2010.